

# Manufacture of 8.4 m off-axis segments: a 1/5 scale demonstration

H. M. Martin<sup>a</sup>, J. H. Burge<sup>a,b</sup>, B. Cuerden<sup>a</sup>, S. M. Miller<sup>a</sup>, B. Smith<sup>a</sup>, C. Zhao<sup>b</sup>

<sup>a</sup>Steward Observatory, University of Arizona, Tucson, AZ 85721, USA

<sup>b</sup>Optical Sciences Center, University of Arizona, Tucson, AZ 85721, USA

## ABSTRACT

We describe the requirements for manufacturing and maintaining alignment of the 8.4 m off-axis segments of the Giant Magellan Telescope's primary mirror, and a demonstration of the manufacturing techniques on the 1.7 m off-axis primary mirror of the New Solar Telescope. This mirror is approximately a 1/5 scale model of a GMT segment. We show that the stressed lap polishing system developed for highly aspheric primary and secondary mirrors is capable of figuring the GMT segments and the NST mirror. We describe an optical test with a null corrector consisting of a tilted spherical mirror and a computer-generated hologram, and derive accuracy requirements for the test. The criterion for accuracy of low-order aberrations is that the active support system can correct any figure errors due to the laboratory measurement, with acceptably small forces and residual errors.

**Keywords:** telescopes, optical fabrication, optical testing, aspheres

## 1. INTRODUCTION

The Giant Magellan Telescope (GMT, Figure 1) is a 22 m telescope whose primary mirror is made of seven 8.4 m circular segments.<sup>1</sup> The segments are lightweight honeycomb sandwich mirrors of the type used for the MMT, Magellan telescopes, and Large Binocular Telescope (LBT). This design makes use of a proven concept for the mirror and supports, and mature manufacturing technology. These are the largest mirrors that can currently be made, so they give the largest collecting area for the natural geometry of seven segments. They guarantee a smooth wavefront over 8.4 m apertures. With adaptive optics using a deformable secondary mirror, segmented to match the primary, the design promises excellent images down to the diffraction limit of a segment, 24 milliarcseconds at  $\lambda = 1 \mu\text{m}$ . Phasing, performed with the secondary mirror segments, will ultimately produce images at the diffraction limit of a 24 m aperture.

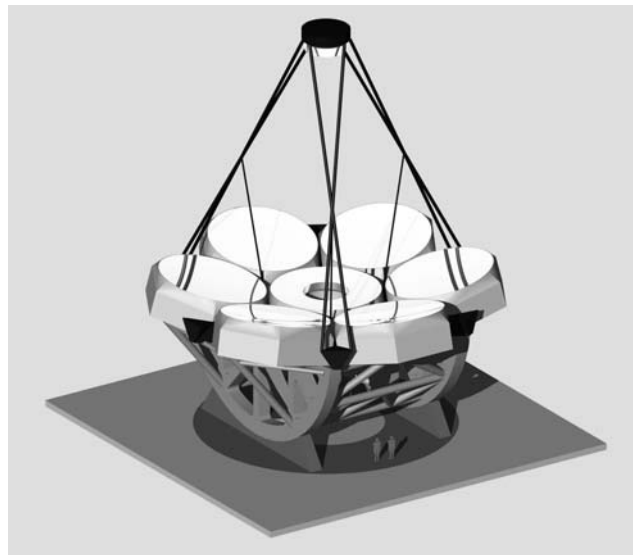


Figure 1. Concept for the Giant Magellan Telescope. The  $f/0.7$  primary mirror consists of seven 8.4 m segments. The adaptive Gregorian secondary, segmented to match the primary, is supported by a lightweight truss.

The primary mirror is fast with an 18 m focal length ( $f/0.7$  over the 25.3 m diameter that includes the full segments). This leads to a compact and stiff telescope structure, with a lightweight truss supporting the adaptive Gregorian secondary mirror. Manufacturing the six off-axis segments is recognized as a challenge. The GMT partners aim to reduce the risk by casting and polishing the first off-axis segment as soon as possible. In addition, the Steward Observatory Mirror Lab and the University of Arizona's Optical Sciences Center are working together to manufacture a 1.7 m off-axis mirror whose optical surface is approximately a 1/5 scale model of a GMT segment. This mirror will be the primary mirror for the New Solar Telescope (NST) at Big Bear Solar Observatory. The NST mirror will be polished and measured using methods that can be scaled directly to the GMT segments.

## 2. MANUFACTURING PLAN FOR 8.4 M SEGMENTS

The GMT segments will be cast, polished and measured at the Steward Observatory Mirror Lab using equipment and techniques that have been developed and refined through manufacture of three 3.5 m mirrors, four 6.5 m mirrors (including those for the MMT and Magellan telescopes), and the two 8.4 m LBT mirrors.<sup>2,3</sup> The GMT segments will have the same internal honeycomb structure as the LBT mirrors and about the same thickness. For the six off-axis segments, the differences relative to the LBT mirror that affect manufacturing are the longer focal length, the lack of a central perforation, and the optical surface with 15 mm peak-to-valley aspheric departure. We will cast each mirror in the spinning furnace, giving the upper surface of the mirror blank the appropriate sag with a best-fit symmetric parabolic surface. The ceramic fiber cores that form the cavities in the honeycomb structure will be sized to follow the final off-axis aspheric surface. When the optical surface is generated to the final asphere, the mirror's front facesheet will be a constant 28 mm thick.

We will generate the GMT segments on the 8.4 m capacity Large Optical Generator used for all the large honeycomb mirrors. This computer-controlled mill, based on a cylindrical polar coordinate system, will create the off-axis optical surface with an accuracy of about 10  $\mu\text{m}$  rms. For symmetric parabolic mirrors, the diamond-impregnated cutting wheel follows a parabolic path as the mirror rotates around its axis. For the off-axis segments, the wheel will be given additional radial motion as the mirror rotates around its mechanical axis (not the optical axis) so that the wheel essentially follows contours of constant height on the asymmetric surface. Because the slope of the optical surface does not exceed 0.12, an error in radial position, due to mechanical backlash or any other source, will produce eight times less surface error than the same error in vertical position.

We will polish the GMT segments on a new 8.4 m capacity machine (Figure 2) equipped with a variety of polishing tools. The machine has two spindles, so two tools can be used simultaneously, or rapid transitions can be made between different tools. The workhorse of the Mirror Lab's polishing program is a 1.2 m diameter stressed lap designed for fast, aspheric mirrors. It changes shape actively to follow the local curvature of the mirror surface. We control figure errors with periods greater than about half the lap diameter using dynamic control of speeds, polishing pressure and pressure gradients. The lap is stiff enough to provide strong passive smoothing of errors with periods less than about 20 cm. The new polisher can use two large stressed laps simultaneously. Alternatively, one of the spindles can be equipped with a 30 cm stressed lap or an orbital polisher with small passive laps of 10-40 cm diameter, either of which will be effective at removing figure errors on scales of 20-60 cm that fall in the gap between figuring and smoothing with the stressed lap.<sup>4</sup>

We will measure the mirror figure with an interferometer at its center of curvature, using a null corrector to produce the aspheric template wavefront.<sup>5</sup> This test will require modification of the Mirror Lab's test tower, which was built to measure mirrors with radii of curvature up to 24 m. The modification required depends on the choice of design for the null corrector. We are considering two options. The first is a scaled-up version of the test we will use for the NST mirror, described in Section 6. It does most of the aspheric compensation by folding the beam with a large tilted spherical mirror, and the rest with a computer-generated hologram (CGH). Because of the folded beam, this test requires little or no extension of the tower, but a redesign of the lower structure to provide clear paths from the interferometer to the folding sphere and from the sphere to the GMT segment. The second option uses an asymmetric refractive null corrector, again with a CGH to remove residual aberrations. The full package is located near the center of curvature, so this test would require a substantial extension of the tower. We are evaluating the two options, including use of the first method for the NST mirror, and will make a decision in time to modify the tower after casting the first GMT segment.



Figure 2. Second 8.4 m LBT primary mirror on the Mirror Lab’s new polishing machine. Loose-abrasive grinding is being performed with a 1.2 m diameter stressed lap. A second spindle, not yet implemented, can drive an identical stressed lap or a smaller tool.

### 3. REQUIREMENTS FOR POLISHING

The GMT segments will be full circular mirrors. Previous GMT design studies considered a closely packed array with a central hexagonal segment and six partial hexagons. The current design with full circular segments was adopted because it maximizes the collecting area and angular resolution, and simplifies the manufacture.

Table 1 lists the dimensions of the off-axis mirror in the current GMT design. The flat rear surface is approximately parallel to the front surface at the center of the mirror. The outer edge is a cylinder whose axis is perpendicular to the rear surface and tilted by  $13.5^\circ$  relative to the optical axis. Viewed from a star, the off-axis aperture is elliptical with an aspect ratio of 1.03.

Table 1. Dimensions of the GMT off-axis mirror segment

radius of curvature	diameter	conic constant	off-axis distance
36 m	8.4 m	-0.9983	8.71 m

The optical surface is over ten times more aspheric than the LBT mirrors, currently the most aspheric large mirrors in a telescope. The stressed-lap polishing system is designed for aspheric surfaces, and it works the same way whether the mirror is symmetric or off-axis. For a symmetric mirror, the lap has a symmetric shape when it is over the center of the mirror and distorts into the appropriate off-axis shape as the polishing motion moves it off the axis. For an off-axis segment, the lap never goes near the center of the parent but otherwise functions in the same way.

There are limits to the curvature changes that can be produced in the lap, so we compare the lap bending required for the GMT segment with that required for the Magellan 6.5 m mirrors and the LBT 8.4 m mirrors. These mirrors were polished to smooth, accurate surfaces with errors on the order of 20 nm rms surface. Table 2 lists the aspheric departures of the Magellan, LBT and GMT mirrors and Table 3 gives the maximum deformation of the stressed lap for each case. The asphericity of the GMT surface is dominated by astigmatism rather than spherical aberration, so the curvature variations across the surface are relatively small, and therefore the lap bending is relatively small as well. Furthermore, as Table 3 shows, the lap bending contains very little coma, the stiffest bending mode. For that reason the

actuator forces required to bend the lap are only about 60% of those needed to bend the lap for the Magellan 6.5 m mirrors. We do not anticipate any difficulty figuring the GMT mirrors with the stressed lap.

Table 2. Peak-to-valley aspheric departure and Zernike polynomial coefficients of the Magellan 6.5 m mirrors and the LBT 8.4 m mirrors. Units are mm and Zernike polynomials are normalized to unity at the edge of the mirror. The peak-to-valley asphericity of the off-axis mirror is approximately  $2|A|+|C|$ .

	Magellan (6.5 m f/1.25)	LBT (8.4 m f/1.14)	GMT off-axis segment
astigmatism ( $A$ )	0	0	-6.56
coma ( $C$ )	0	0	-1.97
spherical aberration	-0.54	-0.92	-0.12
peak-to-valley	0.81	1.38	15.09

Table 3. Peak-to-valley deformation and Zernike polynomial coefficients for a 1.2 m stressed lap used to polish the mirrors of Figure 6. Units are  $\mu\text{m}$  and Zernike polynomials are normalized to unity at the edge of the lap. The peak-to-valley deformation is approximately  $2|F|+|A|+|C|$ .

	Magellan (6.5 m f/1.25)	LBT (8.4 m f/1.14)	GMT off-axis segment
focus ( $F$ )	-212	-213	-276
astigmatism ( $A$ )	-209	-209	-264
coma ( $C$ )	-24	-19	-7
peak-to-valley	657	654	823

The proposed accuracy requirement for the GMT mirrors is given as a structure function. The structure function, defined as the mean square wavefront difference between points in the aperture as a function of their separation, allows different amounts of error on different spatial scales. The specified structure function for the mirror matches the theoretical structure function for seeing in Kolmogorov turbulence, for an image size of 0.11 arcsecond FWHM, with an additional allowance for 2% scattering loss due to small-scale structure. (Image size and scattering loss are specified for  $\lambda = 0.5 \mu\text{m}$ .) The Magellan mirrors satisfied this requirement and the first LBT mirror came within a few percent of meeting it at all scales.

#### 4. REQUIREMENTS FOR TESTING

Accurate measurement of the off-axis aspheric surface is a significant challenge. The measurement requires a template wavefront of the same shape as the ideal mirror surface. This wavefront is produced by a null corrector, which transforms a spherical wavefront into the desired template. Ultimately, the accuracy of the optical surface needs to be about 5 orders of magnitude smaller than the aspheric departure. We anticipate using active optics to achieve this goal: the mirror will be deformed by its 160 active axial supports, with feedback from wavefront measurements in the telescope. The accuracy requirement for the laboratory test then corresponds to the magnitude of correction that can be made with the active support system. This leads to a significant relaxation for a few low-order aberrations like astigmatism. The mirror is flexible in these modes, so they can be corrected in the telescope with little force. They are also the most difficult aberrations to measure accurately in the lab, because small misalignments in the null corrector cause large amounts of these aberrations. For example, the null corrector will put 13 mm peak-to-valley astigmatism in the wavefront by means of a reflection off a tilted sphere (or an equivalent combination of lenses). It will be difficult to align the null corrector to produce the astigmatism to an accuracy better than  $1 \mu\text{m}$  peak-to-valley. We will, however, measure the astigmatism accurately in the telescope, and the active supports can easily bend the mirror by several  $\mu\text{m}$  in astigmatism.

Table 4 lists the magnitudes of several low-order aberrations that can be produced relatively easily with the active supports. These are calculated from a finite-element model of the GMT mirror. The magnitudes are set to satisfy two constraints. First, the correction must require no more than 50 N force for any actuator. Second, the residual surface error must be less than 25 nm rms. We have not yet set precise limits on the maximum correction force or the residual error, but they will be on this order of magnitude, and the values in the table can be scaled when precise limits are chosen. Once these limits are chosen, the aberrations that can be produced set the accuracy requirements for the laboratory measurement.

Table 4. Maximum aberrations that can be produced with active supports, limited by the more stringent of two constraints: maximum correction force < 50 N, and residual surface error < 25 nm rms. Values represents Zernike polynomial coefficients in  $\mu\text{m}$  of surface, with polynomials normalized to unity at the edge of the mirror.

astigmatism	focus	coma	spherical aberration
4.0	0.9	0.5	0.2

The use of active optics only relaxes the accuracy requirements for several low-order aberrations, roughly those listed in Table 4. On smaller scales, the template wavefront must be accurate at a level consistent with the telescope error budget.

While we believe the null corrector can be assembled within tolerances that will satisfy the requirements of Table 4, we also want an independent confirmation of the large-scale accuracy. For symmetric primary mirrors, we have used a CGH that mimics a perfect primary mirror to verify the accuracy of the template wavefront.<sup>6</sup> (In fact, the CGH is expected to be more accurate than the null lens for low-order aberrations, so we use it to calibrate the null lens.) This method will not work for the GMT mirrors because the CGH would have to be larger than anything that can be made to the required accuracy.

We plan to use a scanning pentaprism test for this purpose. The pentaprism directs a beam of about 50 mm diameter parallel to the optical axis, and scans it across the pupil. A detector at the prime focus measures the displacement of the focused spot, which is proportional to the slope error at the illuminated position on the mirror surface. We have developed such a test for a 6.5 m mirror and expect to measure wavefront slopes to a relative accuracy of about 200 nrad, leading to accuracy better than 100 nm in the Zernike coefficients of low-order aberrations. A scanning pentaprism test of the GMT segments will easily reach the accuracies listed in Table 4. A critical part of the test, measuring the position of the detector relative to the mirror segment, will be done with a laser tracker. The laser tracker is a 3-dimensional coordinate measuring machine with a distance-measuring interferometer and two angular encoders. The system tracks and measures the three-dimensional position of a corner cube that is embedded in a steel ball.

Most large mirrors have a loose tolerance on focus, equivalent to a tolerance on radius of curvature of 1 mm or more. The GMT segments have a much tighter tolerance on focus because of the need for all seven mirrors to have the same image magnification. The requirement is strictly that the segments must *match* in radius of curvature rather than that they all have the specified value. While we may be able to achieve better relative accuracy than absolute accuracy in radius, the fact that the mirrors will be made over a period of several years makes it more difficult to maintain a common standard. For the time being we are setting a goal of measuring the absolute radius of curvature to an accuracy such that each segment could be bent to the nominal radius with the active supports.

From Table 4, the allowed adjustment in focus is about 0.9  $\mu\text{m}$  in the Zernike coefficient for surface error, equivalent to a change in radius of curvature of about 0.3 mm. We have measured the LBT radius (19.2 m) to an accuracy of 0.5 mm with a calibrated steel tape. We have two options for the GMT radius measurement. The first is the same scanning pentaprism measurement that will be used to measure astigmatism, coma and spherical aberration. This test measures the focus error directly and requires measurement of the axial position of the detector to better than 0.15 mm (half the tolerance in radius of curvature). The second method is to use a laser tracker as a profilometer, scanning the ball across the optical surface. The tracker measures absolute distance to better than 0.1 mm, and measures changes in distance to about 1  $\mu\text{m}$ . The most difficult part of the radius measurement is the direct measurement of the focus error, i. e., the sag of the mirror surface. We have demonstrated a relative accuracy of better than 2  $\mu\text{m}$  rms for points on the surface of a 1.8 m spherical mirror, measured from the vicinity of its center of curvature so that only the distance measurement (as opposed to the angular measurements) is critical. Such accuracy will be adequate to measure the

Zernike focus coefficient to  $0.9 \mu\text{m}$  if we can maintain stability of the system—the mirror and laser tracker—over the duration of the measurement. We will test this technique on the 1.7 m NST mirror.

## 5. ALIGNMENT REQUIREMENTS

Alignment tolerances are relatively tight for the GMT because of the  $f/0.7$  primary mirror. Optical alignment should be held to an accuracy that does not degrade image quality in any observing mode, from relatively simple ground-layer adaptive optics—correcting with only the deformable secondary mirror—to the most ambitious multi-conjugate or extreme adaptive optics whose goal is full diffraction-limited imaging. In all modes, the primary mirror segments must be positioned with sufficient resolution that residual alignment aberrations are a fraction of those caused by the atmosphere, and maintain this level over wavefront averaging intervals of about 1 minute. The aberrations will be measured in the wavefront and the immediate correction will be made with the adaptive secondary mirror, but the correction should not be allowed to be a large fraction of the correction needed for seeing.

Table 5 lists the coefficients of low-order aberrations resulting from misalignment of the off-axis segments, and for comparison the rms values of these coefficients due to the atmosphere in  $0.25$  arcsecond FWHM seeing. Aberrations due to translation and rotation of segments are derived from Lubliner and Nelson<sup>7</sup>. Aberrations due to seeing are derived from Noll<sup>8</sup> assuming Kolmogorov turbulence with no outer scale. Lateral translation of the symmetric central segment causes only coma, with the same sensitivity given in Table 5.

Table 5. Sensitivity to misalignment for an off-axis GMT segment. Values are Zernike coefficients of wavefront error in nm, evaluated over a single mirror. Zernike polynomials are normalized to  $\pm 1$  at the edge of the mirror. Values listed for  $0.25''$  seeing represent the rms variation of the Zernike coefficient due to seeing. Orientations of aberrations refer to the position of the maximum wavefront error, relative to the direction to the optical axis. A translation of  $100 \mu\text{m}$  in the tangential direction is equivalent to a rotation of approximately  $\pm 50 \mu\text{m}$ .

aberration	tip-tilt of $\pm 1 \mu\text{m}$ at edge	$100 \mu\text{m}$ radial translation	rotation of $\pm 50 \mu\text{m}$ at edge	$0.25''$ seeing
tilt	2000			1336
focus		330		262
astigmatism at $0^\circ$		330		372
astigmatism at $45^\circ$			340	372
coma at $0^\circ$		50		222
coma at $90^\circ$			50	222

Very different tolerances and time scales apply to in-plane and out-of-plane motion of the primary mirror segments. Table 5 shows that in-plane motion causes significant aberrations for displacements of tens of microns. These motions can be controlled with low resolution based on the measured wavefront error, averaged for a minute or more. The LBT hard-point control system has a resolution of about  $1 \mu\text{m}$  and a bandwidth of about  $1 \text{ Hz}$ , more than adequate to control the in-plane motion.

Out-of-plane motion must be controlled at the level of microns (for ground-layer adaptive optics observations) to tens of nm (for diffraction-limited observations). Wind buffeting will cause significant perturbations on a timescale of about 1 second. Tip-tilt will be sensed with the Shack-Hartmann wavefront sensor while all out-of-plane segment motions will be sensed with a combination of optical edge sensors and an interferometric phasing camera.

All aberrations due to both in-plane and out-of-plane motion will be corrected automatically by the adaptive secondary mirror on a time scale of milliseconds. Slowly varying components will be off-loaded to the primary mirror segments on a time scale of seconds to minutes. This slow adjustment of the primary segments will include rigid-body motion and shape control. The control loop for primary segment shape and alignment and telescope alignment runs at a rate on the order of  $0.01 \text{ Hz}$ . The average wavefront measurement provides feedback for a series of corrections: secondary mirror alignment, primary segment alignment, and primary segment shape. The corrections will be derived

from the deformable secondary mirror commands; its time-averaged displacements provide the feedback for alignment and primary segment shape. The slow active optics control loop consists of the following steps:

1. Measure the wavefront with the Shack-Hartmann wavefront sensor, averaged over a minute or more, or through the time-averaged displacements of the deformable secondary.
2. Fit global focus and coma over the 24 m aperture. Correct by repositioning the secondary mirror.
3. Fit alignment error for each primary mirror segment. The fit is based on the signature aberrations of each alignment degree of freedom. Correct by repositioning each segment hexapod.
4. Fit 10 or more bending modes for each primary segment. Correct by adjusting the segment support forces.

## 6. A 1/5 SCALE DEMONSTRATION

Most of the fabrication and measurement techniques that we will use for the GMT mirrors will be demonstrated on a smaller scale with the 1.7 m NST primary mirror. Its dimensions are listed in Table 6. The optical surface is nearly a 1/5 scale model of the GMT surface, and its asphericity is 2.7 mm peak-to-valley surface. The mirror is 100 mm thick, solid Zerodur. The aspheric surface has been generated to an accuracy of 10  $\mu\text{m}$  rms by Kodak. We will polish it with a 2 m polishing machine equipped with a 30 cm diameter stressed lap, essentially the same system used to polish the 1.8 m f/1 primary mirror of the Vatican Advanced Technology Telescope and secondary mirrors for the 3.5 m ARC telescope, 2.5 m Sloan Digital Sky Survey telescope, MMT (three secondaries) and currently the LBT (two secondaries). As is the case for the GMT 8.4 m segments, the asphericity of the NST mirror has a large amplitude but is dominated by astigmatism and coma rather than spherical aberration, so the bending of the stressed lap is actually less than the bending required for several of the secondary mirrors that have been figured to high accuracy.

Table 6. Dimensions of the NST off-axis mirror

radius of curvature	diameter	conic constant	off-axis distance
7.7 m	1.7 m	-1	1.84 m

Testing is the major challenge for the NST mirror. The main optical test is an interferometric center-of-curvature test shown in Figure 3.<sup>5</sup> The null corrector comprises a tilted spherical mirror that compensates most of the asphericity (mostly astigmatism) and a CGH that compensates the residual asphericity and provides system alignment references. This test is scalable to the GMT size, but the 0.5 m sphere becomes a much more challenging 2.5 m sphere. In both cases the figure of the sphere will be measured from its center of curvature, and the measurement of the off-axis primary will be corrected for errors in the sphere. The 70 mm diameter hologram cannot simply be scaled up by a factor of 5, because there is no equipment capable of writing an accurate hologram on such a large substrate, so the GMT version will require an additional element to re-image the CGH pattern.

The accuracy of the null corrector depends on its internal alignment. The most demanding tolerance is the position of the spherical mirror relative to the hologram, which must be controlled to better than 10  $\mu\text{m}$ . In addition to the main hologram pattern that compensates the residual asphericity in the test wavefront, the hologram contains a number of other patterns, written on different parts of the substrate, that guide the alignment. Some of these patterns focus light onto tooling balls that define the position of the spherical mirror; these return null wavefronts to the interferometer when the mirror is in the correct position. Another pattern returns a null wavefront to the interferometer when the hologram and focusing lenses are aligned relative to the interferometer. Another set of patterns produce crosshair images at known locations on the primary mirror; these are used to determine the distance and clocking angle of the mirror relative to the optical axis.

To corroborate the center-of-curvature test of the NST primary, we will perform an autocollimation test with an interferometer at the focus of the off-axis paraboloid and a large flat mirror perpendicular to the optical axis. This test cannot be scaled to an 8.4 m mirror, but the pentaprism test described earlier synthesizes the autocollimation test by producing a set of parallel beams across several diameters of the 8.4 m mirror.

The null test described above can be used on a polished surface whose accuracy is no worse than a few waves, so the interference fringes can be resolved over the full image of the mirror. We need a different measurement to guide us through loose-abrasive grinding when the surface is neither specular nor accurate enough for the null test. An infrared version of the same null test is difficult to implement because of the hologram's strong sensitivity to wavelength, which is uncertain at a significant level in a  $10.6\ \mu\text{m}$   $\text{CO}_2$  laser. For the NST mirror, we will measure the shape of the ground surface with a laser tracker, sampling 20-40 points on the surface. We have demonstrated measurement accuracy of 1-2  $\mu\text{m}$  rms for a 1.8 m spherical mirror, with restrictions on the measurement geometry described in Section 4. This will be adequate to make the transition to the visible null test provided we achieve the same accuracy on the aspheric surface.

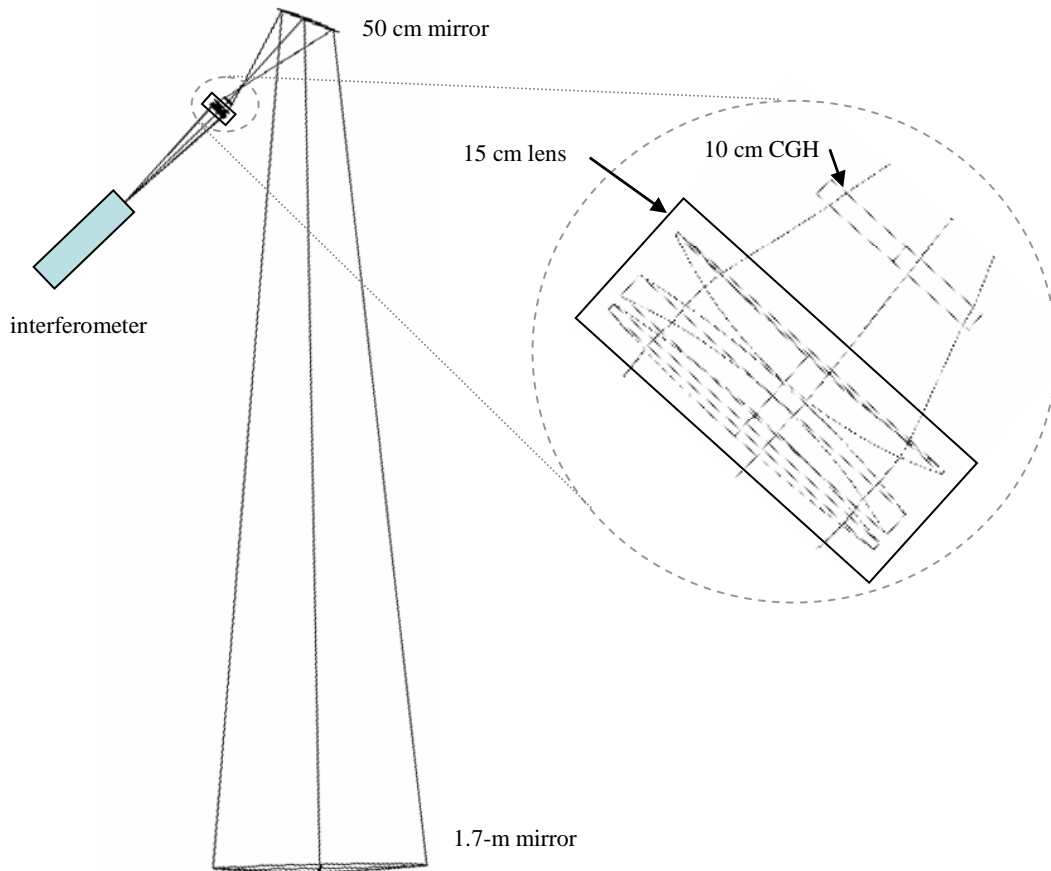


Figure 3. Optical test of NST off-axis primary mirror. The null corrector consists of a tilted 0.5 m spherical mirror and a computer-generated hologram.

## 7. CONCLUSIONS

We have defined the requirements for manufacturing the 8.4 m off-axis segments of the GMT primary mirror, and developed processes and designs that appear capable of meeting these requirements. The most challenging aspect of the manufacturing process is accurately measuring the extremely aspheric surface. We have a promising design for the interferometric measurement with a null corrector, and for a supplementary measurement to verify the accuracy of low-order aberrations that are most sensitive to misalignment of the null corrector. We will demonstrate both polishing and measuring techniques through the manufacture of the 1.7 m off-axis NST primary mirror.

We have analyzed the requirements for alignment of the GMT segments in the telescope. Rapid correction of all wavefront errors will be made with the adaptive secondary mirror, and slowly varying errors due to alignment will be

transferred to the primary mirror segments. Tolerances for in-plane motion of the segments are loose compared with the resolution of the segments' hard-point positioners.

## ACKNOWLEDGEMENTS

This work has been supported by the Air Force Office of Scientific Research, the National Science Foundation, and the New Jersey Institute of Technology.

## REFERENCES

1. R. Angel, J. Burge, J. L. Codona, W. Davison and B. Martin, "20 and 30 m telescope designs with potential for subsequent incorporation into a track-mounted pair (20/20 or 30/30)", in *Future Giant Telescopes*, ed. J. R. P. Angel and R. Gilmozzi, SPIE 4840, p. 183 (2003).
2. H. M. Martin, J. R. P. Angel, J. H. Burge, S. M. Miller, J. M. Sasian and P. A. Strittmatter, "Optics for the 20/20 Telescope", in *Future Giant Telescopes*, ed. J. R. P. Angel and R. Gilmozzi, SPIE 4840, p. 194 (2003).
3. H. M. Martin, R. G. Allen, J. H. Burge, L. R. Dettmann, D. A. Ketelsen, S. M. Miller and J. M. Sasian, "Fabrication of mirrors for the Magellan Telescopes and the Large Binocular Telescope", in *Large Ground-based Telescopes*, ed. J. M. Oschmann and L. M. Stepp, Proc. SPIE 4837, p. 609 (2003).
4. H. M. Martin, R. G. Allen, B. Cuerden, S. T. DeRigne, L. R. Dettmann, D. A. Ketelsen, S. M. Miller, G. Parodi and S. Warner, "Primary mirror system for the first Magellan telescope", in *Optical Design, Materials, Fabrication, and Maintenance*, ed. P. Dierickx, Proc. SPIE 4003, p. 2 (2000).
5. J. H. Burge, H. M. Martin, J. Sasian, R. Zehnder, C. Zhao, "Interferometric metrology for the Giant Magellan Telescope", in these proceedings.
6. J. H. Burge, D. S. Anderson, D. A. Ketelsen, S. C. West, "Null test optics for the MMT and Magellan 6.5-m f/1.25 primary mirrors", in *Advanced Technology Optical Telescopes V*, ed. L. M. Stepp, Proc. SPIE 2199, p. 658 (1994).
7. J. Lubliner, J. E. Nelson, "Stressed mirror polishing. 1: A technique for producing nonaxisymmetric mirrors", *Applied Optics*, Vol. 19, p. 2332 (1980).
8. R. J. Noll, "Zernike polynomials and atmospheric turbulence", *J. Opt. Soc Am.*, Vol. 66, p. 207 (1976).